Cavity Optomechanics with Anderson-Localized Optical Modes

G. Arregui,[1,2] R. C. Ng,[1] M. Albrechtsen,[2] S. Stobbe,[2] C. M. Sotomayor-Torres,[1,3] and P. D. García[1,*]
[1]Catalan Institute of Nanoscience and Nanotechnology (ICN2), CSIC and The Barcelona Institute of Science and Technology, Campus UAB, Bellaterra, 08193 Barcelona, Spain
[2]DTU Electro, Department of Electrical and Photonics Engineering, Technical University of Denmark, Ørsteds Plads 343, Kgs. Lyngby, DK-2800, Denmark
[3]ICREA—Institució Catalana de Recerca i Estudis Avançats, 08010 Barcelona, Spain

(Received 27 July 2022; accepted 16 December 2022; published 25 January 2023)

Confining photons in cavities enhances the interaction between light and matter. In cavity optomechanics, this enables a wealth of phenomena ranging from optomechanically induced transparency to macroscopic objects cooled to their motional ground state. Previous work in cavity optomechanics employed devices where ubiquitous structural disorder played no role beyond perturbing resonance frequencies and quality factors. More generally, the interplay between disorder, which must be described by statistical physics, and optomechanical effects has thus far been unexplored. Here, we demonstrate how sidewall roughness in air-slot photonic-crystal waveguides can induce sufficiently strong backscattering of slot-guided light to create Anderson-localized modes with quality factors as high as half a million and mode volumes estimated to be below the diffraction limit. We observe how the interaction between these disorder-induced optical modes and in-plane mechanical modes of the slotted membrane is governed by a distribution of coupling rates, which can exceed $g_o/2\pi \sim 200$ kHz, leading to mechanical amplification up to self sustained oscillations via optomechanical backaction. Our Letter constitutes the first steps towards understanding optomechanics in the multiple-scattering regime and opens new perspectives for exploring complex systems with a multitude of mutually coupled degrees of freedom.

DOI: 10.1103/PhysRevLett.130.043802

The presence of thermally excited vibrations in solid-state materials modifies light-matter interaction [1,2], which often leads to undesirable effects such as the dephasing of single photons emitted by self-assembled quantum dots [3] or optical beam jitter in interferometric gravitational-wave detectors [4]. When properly controlled, this same interaction facilitates ground-breaking applications such as ultrafast laser spectroscopy [5] and passive radiative cooling [6], while offering fundamental insight into open challenges such as quantum gravity [7], among other quantum technological applications [8]. A conventional method to enable such control is through enhancement of the optomechanical interaction by simultaneously confining the electromagnetic and displacement fields within the same carefully nanostructured volume [9]. In theory, material and geometry provide very fine control over the parameters governing the dynamics of such optomechanical systems. In practice, they are challenging to realize exactly as designed due to unavoidable fabrication disorder which compromises the governing parameters (notably, the quality factor Q of the optical cavity) [10]. Generally, the strategy to limit disorder-mediated losses is to improve nanofabrication, but a certain level of disorder is unavoidable [11]. Here, we take an alternative route to cavity optomechanics which deliberately exploits unavoidable sidewall roughness in a suspended slot photonic-crystal waveguide to mediate the coupling between infrared photons and acoustic phonons. The subwavelength confinement near the dielectric air-silicon interfaces simultaneously enables efficient coupling of the slot-confined light to in-plane mechanical motion, while promoting scattering due to slot sidewall surface roughness. In the slow light regime [12], where both effects are enhanced [13,14], backscattering induces high-Q random localized optical cavities; i.e., Anderson-localized modes [15,16], that efficiently couple to the in-plane mechanical motion of the slotted membrane over a wide frequency range.

The waveguides we explore are suspended silicon photonic-crystal waveguides with an air slot of width s along the waveguide axis and fabricated in silicon-on-insulator substrates [Fig. 1(a)]. They support a guided mode along the defect that exhibits subwavelength light confinement within the air slot while slowing light down with a very large group index, $n_g = c/|v_g|$, at the Brillouin zone edge [Fig. 1(b)]. The fabricated waveguides (Supplemental Material, Sec. S2 [17]) are affected by line-edge roughness along the etched silicon sidewalls, which produces stochastic fluctuations $\delta s(x)$ of the slot width [Fig. 1(c)]. This gives rise to extrinsic out-of-plane and backscattering [29], both of which are enhanced in the slow-light regime and at air-dielectric interfaces with intense fields [30], as is the

case at the air-slot boundaries. In an infinite waveguide, coherent multiple backscattering leads to interference effects that spectrospatially localize the field in a quasi-one-dimensional manifestation of Anderson localization [31]. In practice, this localization occurs when the waveguide length L is larger than the localization length ξ [32], which can be very short at high n_g (Supplemental Material, Sec. S1. 2 [17]). Therefore, disorder-induced cavities occur over a narrow wavelength range around the waveguide cutoff, whose extent is determined by ξ/L. Figure 1(d) depicts the electromagnetic field for a characteristic delocalized and Anderson-localized modes in a waveguide ($L = 60a$) accounting for slot line-edge roughness, modeled as exponentially correlated normally distributed fluctuations with rms amplitude $\sigma = 3$ nm (Supplemental Material, Sec. S1. 2 [17]). We compute the effective mode volume of the localized mode in Fig. 1(d) to be $V_{\mathrm{eff}} \sim \lambda^3/100$ (Supplemental Material, Sec. S3. 2 [17]). The tight confinement below the diffraction limit results from a combination of: (i) light being squeezed into the slot in the propagating Bloch mode with unit-cell effective mode volumes, $V_{\mathrm{eff,cell}}$, down to $\lambda^3/250$, and (ii) being localized along the waveguide to a length scale given by ξ.

We confirm the presence of wavelength-scale Anderson-localized modes by far-field imaging measurements [33] of waveguides embedded into photonic circuits (dark field optical microscope image in Fig. 1(e)). Light is coupled into a strip waveguide using a broadband grating coupler [34] (blue) then transferred into a slot waveguide with a strip-to-slot mode converter [35] (purple) and subsequently interfaced with the slot photonic-crystal waveguide of length L (red). The color map in Fig. 1(f) shows the wavelength-dependent signal obtained from a near-infrared camera along the waveguide axis for wavelengths around the cutoff observed in the circuit transmission ($\lambda \sim 1538$ nm), shown to the right of the color map. The map reveals the presence of intense spectrospatially localized scattered fields, indicating the formation of cavities with a spatial extent that decreases towards the cutoff. The most extended mode (v) results in a small resonant peak in transmission while more localized modes (i)–(iv) do not appear in transmission. In this set of waveguides, the most localized mode exhibits a single Gaussian-like hot spot of width $\sim 4a$ [Fig. 1(g)] and an intrinsic quality factor $Q_i \sim 2.8 \times 10^5$. The effective volume of this mode is estimated to be $V_{\mathrm{eff}} \sim \lambda^3/50$ by assuming that the far field

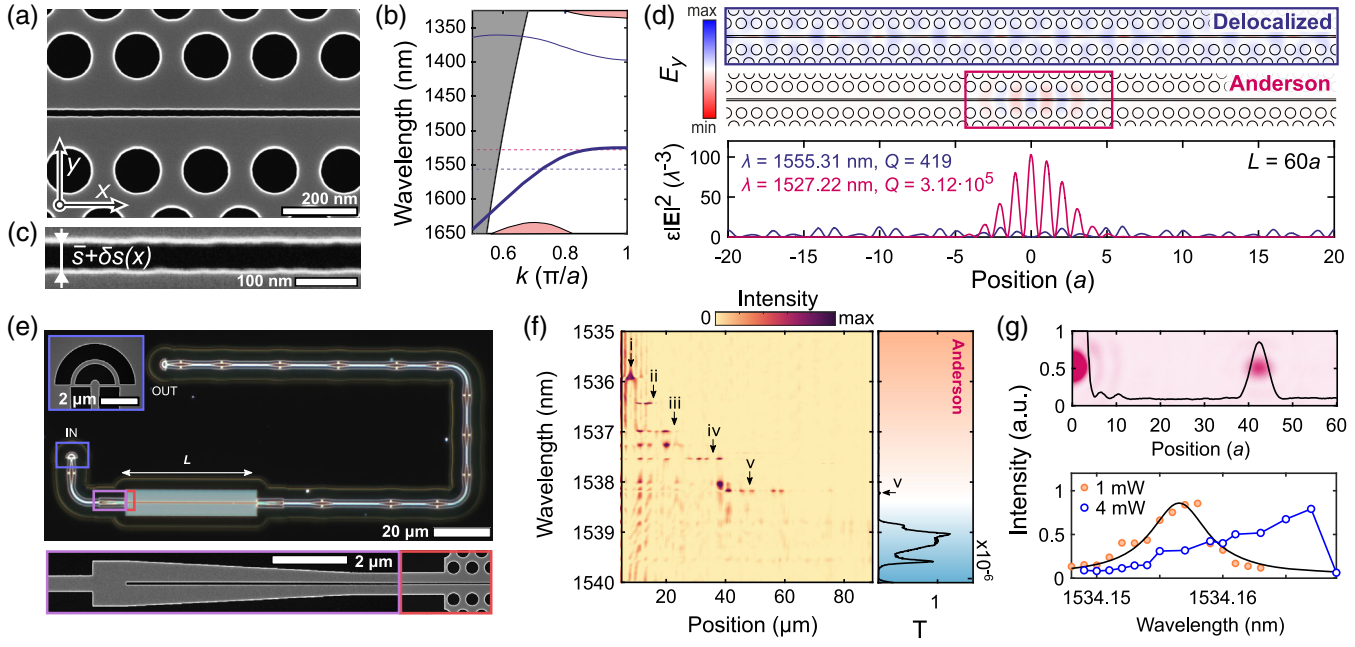

FIG. 1. Anderson localization of light in an air slot photonic-crystal waveguide. (a) Scanning electron microscopy (SEM) micrograph of the explored waveguide and its (b) transverse-electric-like band structure. Geometric parameters are periodicity $a = 450$ nm, radius $r = 155$ nm, slot width $s = 52$ nm, and membrane thickness $t = 220$ nm. (c) SEM of an etched slot of width $s = 52 + \delta s(x)$ nm, with $\delta s(x)$ given by the sidewall line-edge roughness. (d) Simulated $E_y(x, y, z = 0)$ of a typical delocalized (blue box) and an Anderson-localized mode (pink box) under 3 nm rms slot line-edge roughness (top). The normalized energy density along the slot axis (bottom). (e) Dark-field microscope image showing the tested photonic circuits consisting of free-space grating couplers (blue), strip-to-slot converters (purple), and slot waveguide to photonic-crystal waveguide interfaces (red). (f) Spectrospatial mapping of the scattered far fields measured in a $\bar{s} = 52$ nm, $L = 300a$ waveguide using a NIR camera and optical transmission measured at the output grating coupler. (g) Spatially (top) and spectrally (bottom) resolved far-field of a wavelength-scale Anderson-localized mode with estimated $V_{\mathrm{eff}} \sim \lambda^3/50$ and extracted $Q = Q_i = 2.77 \times 10^5$. The latter is obtained from a Lorentzian fit (black line) to the measured intensity (orange dots).

is proportional to the near-field envelope of the cavity mode and by using the value for $V_{\mathrm{eff,cell}}$ given previously (Supplemental Material, Sec. S3. 1 [17]). This estimation agrees well with simulated values of V_{eff} [Fig. 1(d)], and leads to a $Q_{\mathrm{i}}/V_{\mathrm{eff}} \sim 1.5 \times 10^7 \lambda^{-3}$, among the highest values ever reported for an optical cavity [36].

As shown in the spectral map of Fig. 1(f), butt coupling from an integrated access waveguide only allows the excitation of localized modes at a distance of approximately the localization length ξ from the input. We circumvent this limitation with a tapered fiber loop placed in contact with the structure along the waveguide axis [37]. The waveguides are terminated by a photonic crystal which creates long cavities [Fig. 2(a) and Supplemental Material, Sec. S1. 2 [17]] that we denote as SLN cavities [38] and that allow for mapping of the waveguide dispersion relation [39]. Evanescent coupling to resonant modes appear here as sharp spectral dips in the transmitted optical signal [the top panels of Figs. 2(b) and 2(c)]. The strong dispersion of $\xi(\lambda)$ [40] leads to two transport regimes. When $\xi(\lambda) \gg L$, light travels quasiballistically building up Fabry-Pérot (FP) modes with resonant wavelengths determined by the waveguide group index $n_{\mathrm{g}}(\lambda)$ and the cavity length L. When $\xi(\lambda) \ll L$, backscattering leads to the formation of Anderson-localized modes with randomly distributed resonant wavelengths and strong mode-to-mode variations in the coupled fraction (Supplemental Material, Sec. S4. 4 [17]). The free spectral range in the FP region is used to reconstruct the group index of the slot band, $n_{\mathrm{g,exp}}(\lambda)$ [Figs. 2(b) and 2(c) and Supplemental Material, Sec. S4. 3 [17]]. Below a certain value of n_{g}, we observe close agreement between the simulated $n_{\mathrm{g,sim}}(\lambda)$ and the reconstructed $n_{\mathrm{g,exp}}(\lambda)$. Above a certain value of n_{g}, localization leads to strong fluctuations of $n_{\mathrm{g,exp}}(\lambda)$ around $n_{\mathrm{g,sim}}(\lambda)$. The exact crossover between the two transport regimes depends on L [41], occurring at lower n_{g} for longer waveguides. For the longest cavity waveguides ($L = 300a$), we observe multiple high-Q localized modes in a ~10 nm range around the cutoff wavelength. Figure 2(d) shows the optical transmission associated with the highest intrinsic quality factor, Q_{i}, observed in a waveguide with $\bar{s} = 52$ nm. Figure 2(e) shows the histogram of Q_{i} as obtained from single-position measurements in 11 nominally identical waveguides. Most of the observed modes have $Q_{\mathrm{i}} > 10^5$, in agreement with the few modes observed via the far-field measurements of Fig. 1(f), but local probing of modes deep within the waveguide gives access to the full distribution. The histogram is well fitted with a log-normal distribution, showing the expected behavior deep within the localization regime [42,43]. We measure similar distributions for all $\bar{s} > 30$ nm, with even higher values observed for wider slots (Supplemental Material, Sec. S4. 5 [17]). The values of Q measured with the loop and the values of V_{eff} estimated from the far-field images highlight the potential of such disorder-induced cavities not only for cavity quantum electrodynamics experiments with trapped atoms [44], where the ultrahigh $Q_{\mathrm{i}}/V_{\mathrm{eff}}$ achieved here would naturally emerge, but also for nonlinear optics [45], sensing [46], and cavity optomechanics.

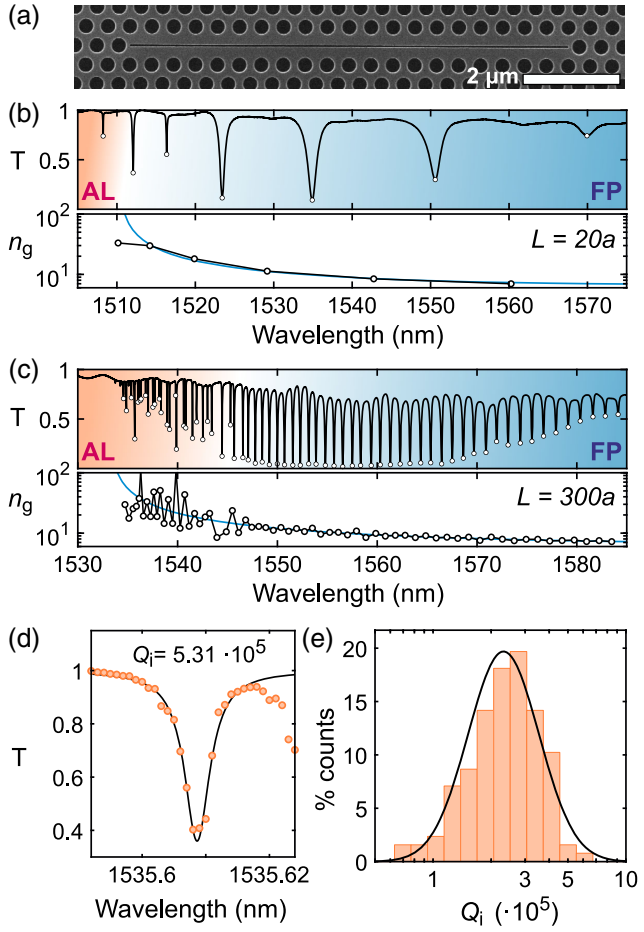

FIG. 2. Evanescent coupling to Anderson-localized optical modes. (a) SEM of a $\bar{s} = 52$ nm, $L = 20a$ mirror-terminated slot photonic-crystal waveguide. A tapered fiber loop is placed on top of the waveguide to couple into the cavity modes. (b) Optical transmission spectrum of the structure shown in (a) and comparison of the reconstructed $n_{\mathrm{g,exp}}(\lambda)$ (black line) and simulated $n_{\mathrm{g,sim}}(\lambda)$ group indices (blue line). (c) Same as (b) for $L = 300a$. Both (b) and (c) exhibit a crossover between ballistic transport forming Fabry-Pérot resonances (shaded blue) to Anderson-localized modes (shaded orange). The free spectral range varies monotonously in the FP region but is randomized in the Anderson-localization region. (d) Optical spectrum of the highest intrinsic quality factor, Q_{i}, Anderson-localized mode. (e) Histogram of Q_{i} for the Anderson-localized modes measured for $\bar{s} = 52$ nm, $L = 300a$, fitted to a log-normal distribution (black line).

Engineered heterostructure cavities in similar waveguides have been shown to be excellent mechanical displacement sensors for mechanical modes that produce changes Δs in slot width [47–49]. Here, we employ disorder-induced cavity modes to transduce the motion of multitude breathing in-plane mechanical modes [fundamental mode shown in Fig. 3(a)]. We drive the cavity

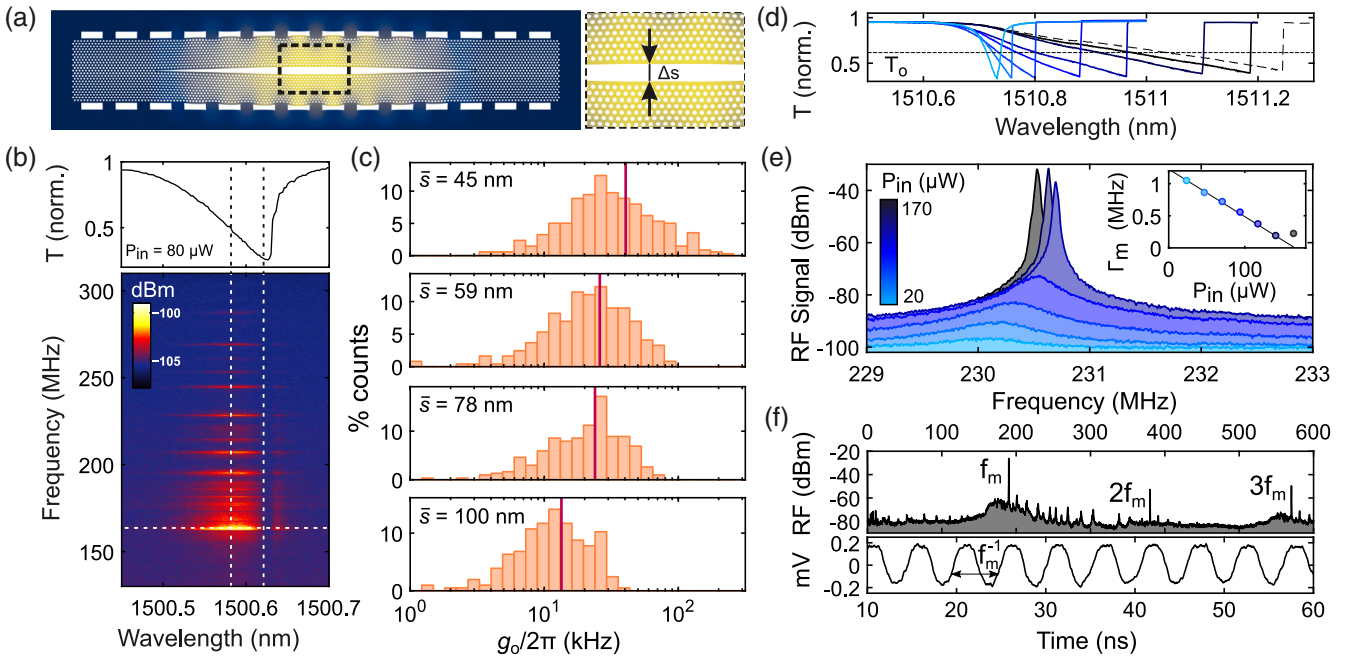

FIG. 3. Optomechanical interaction in the Anderson-localization regime. (a) Fundamental in-plane mechanical mode for an SLN cavity of length $L = 50a$. The inset shows the local variation of the slot width Δs in the center. (b) Characteristic wavelength-resolved (top) optical transmission and (bottom) radio frequency spectrum driving an Anderson-localized mode in a $\bar{s} = 78$ nm and $L = 145$ μm SLN cavity. The thermally active mechanical modes appear as horizontal lines, with the fundamental mode in (a) highlighted with a dashed line. The vertical dashed lines identify the points of maximum and vanishing transduction. (c) Histogram of the vacuum optomechanical coupling rate, g_o, in the Anderson-localization regime as a function of slot width $\bar{s}$. The average value in each histogram is indicated with a vertical line. (d) Optical transmission spectrum across an Anderson-localized mode as a function of P_{in}. The dashed line indicates the coupled fraction, T_o, at which the radio frequency spectra in (e) are acquired. The inset to (e) shows the effective mechanical linewidth, Γ_m^{eff}, measured as a function of P_{in} (blue dots) along with a linear fit (black line) used to extract g_o. (f) Characteristic (top) rf spectrum and (bottom) time-resolved transmission of the optomechanical system undergoing coherent self-sustained oscillations.

modes and measure the transduced radio frequency (rf) modulation while scanning the laser wavelength across the optical resonance. A characteristic optical transmission and associated rf spectral map are shown in Fig. 3(b). Horizontal peaks in the color map originate from the thermal motion of mechanical eigenmodes of the membrane, all with mechanical linewidths of $\Gamma_m/2\pi \sim 1$ MHz. The most intense peak in the spectrum occurs at $\Omega_m/2\pi = 161$ MHz, the frequency of the fundamental in-plane breathing mechanical mode for $L = 300a$ (Supplemental Material, Sec. S5 [17]). Vertical dashed lines denote wavelengths of maximum and no mechanical transduction. The wavelength dependence of the rf signal indicates a dispersive optomechanical coupling between the probed optical mode and the mechanical modes, an observation common to all probed Anderson modes. We therefore quantify the coupling between photon-phonon pairs by the vacuum optomechanical coupling rate, g_o, which we measure by driving the optical cavities with a known phase-modulated signal [50] (Supplemental Material, Sec. S6 [17]). The histograms of g_o for different values of $\bar{s}$ are shown in Fig. 3(c). We find maximum values around 200 kHz, comparable to their engineered counterparts [47–49,51], and the average of g_o (vertical line) is found to increase for narrower air slots. This has been reported in conventional cavities [52,53], where g_o is accurately estimated from the field envelope, which depends weakly on $\bar{s}$, and the unit cell optomechanical coupling, $g_{o,cell}$ [54], which grows exponentially with decreasing s (Supplemental Material, Sec. S1. 1 [17]). We observe the same trend here even if the field extension along the waveguide, statistically given by ξ, may strongly depend on $\bar{s}$ through $\bar{s}$-dependent scattering cross sections [14] or enhanced line-edge roughness for smaller widths [55], which we observe in SEM images. However, the localization length ξ drops down to only a few unit cells over a broad range of n_g regardless of $\bar{s}$. Therefore we also attribute the observed trend in Fig. 3(c) to that of $g_{o,cell}$. The larger reduction of g_o observed between $\bar{s} = 78$ and $\bar{s} = 100$ nm originates from weaker localization due to the angled sidewalls promoting scattering into a nearly phase-matched transverse-magnetic-like band (Supplemental Material, Secs. S2 and S4. 5 [17]). We note that control over the sidewall roughness δs via intentional disorder will most likely also decrease ξ [31], leading to weaker coupling strengths as well as reduced Q factors.

The measured figures of merit allow for dynamical backaction in the Anderson-localization regime, albeit only mechanical amplification since red-detuned driving is prevented by increasing thermo-optic shifts at increasing powers [Fig. 3(d)]. We acquire rf spectra at varying power P_{in} and fixed laser-cavity detuning, Δ, selected by measuring at a fixed transmittance, T_{o}, an approach that neglects any nonlinear optical losses. This results in a tuning of the mechanical frequency, a reduction of the mechanical linewidth, and an increase of the amplitude vibration, as shown for a mode with $\Omega_{\mathrm{m}}/2\pi = 230$ MHz in Fig. 3(e). We observe the effective linewidth including optomechanical damping, $\delta\Gamma_{\mathrm{om}}$, to depend linearly with P_{in} [9] and extract $g_{\mathrm{o}}/2\pi = 228 \pm 7$ kHz from the slope [Fig. 3(e) inset]. This value is slightly larger than the one obtained using the phase-modulation technique, which indicates that other physical processes may contribute to the backaction [53,56]. When $\delta\Gamma_{\mathrm{om}} \approx -\Gamma_{\mathrm{m}}$, the optomechanical system reaches a regime of self-sustained oscillations, where $\Gamma_{\mathrm{m}}^{\mathrm{eff}}$ saturates [57]. For the mode studied in Fig. 3(e), this occurs at $P_{\mathrm{in}} \sim 150$ μW. The coherently amplified mechanical oscillation in the frequency and time domains at a power $P_{\mathrm{in}} = 200$ μW, above the lasing threshold, is shown in Fig. 3(f). The wide rf spectrum exhibits multiple harmonics of the lasing mode, and the self-triggered temporal trace is the fingerprint of the coherent nature of the motion. Note that the mechanical frequency of the lasing mode is $\Omega_{\mathrm{m}}/2\pi = 190$ MHz, unlike in Fig. 3(e). This indicates sideband unresolved ($\Omega_{\mathrm{m}}/\kappa = 10^{-2}$–$10^{-1}$) mechanical mode competition between mechanical modes with comparable Γ_{m} and g_{o} to the driven cavity. Mechanical lasing initially occurs for the mode with lowest threshold [Fig. 3(e)], but, once above threshold for two or more modes, that with the largest g_{o} is amplified [Fig. 3(f)].

In recent years, well-known functionalities such as cavity quantum electrodynamics [58,59], lasing [60], imaging [61], sensing [62], or computing [63] have been explored in systems where structural imperfection plays a primary role. Here, we use the roughness in a slow-light air-slot photonic-crystal waveguide for cavity optomechanics by confining light into high quality factor and small mode volume Anderson modes that couple to and amplify the mechanical eigenmodes of the system, achieving self-sustained coherent mechanical oscillations at sub-mW optical powers. From a practical perspective, the Anderson modes explored here and their coupling to motion will help elucidate the role of surface roughness in nano-opto-electro-mechanical systems that employ deep subwavelength air slots to control the flow of light. More fundamentally, our Letter constitutes a step forward in unraveling the intricate connection between optical pressure and light transport in the multiple-scattering regime [64], the physics of which will dominate as photonic nanocavity research approaches length scales on the order of the roughness [65]. Owing to the unprecedented light-matter interaction figure of merit estimated of at least $Q_{\mathrm{i}}/V_{\mathrm{eff}} \sim 1.5 \times 10^{7}\lambda^{-3}$, and the air-confined nature of the involved optical modes, it opens the door to optical excitations with free-electron beams [66] as well as photon-phonon interactions mediated by trapped atoms [67]. In addition, the structure we present is a versatile multimode optomechanics platform to study mechanical mode competition leading to mode hopping [68] and anomalous cooling [69], many-mode phonon lasing [70,71], and cascaded mechanical state transfer [72]. While the mechanical modes explored here are membrane-like modes, simultaneous wave guiding of GHz slow sound [73] and telecom slow light is possible in a slotted optomechanical waveguide [74] that uses shamrock-shaped holes [75]. This will enable the generation of guided GHz coherent acoustic phonons directly from a waveguide [74] as well as the exploration of acoustic Anderson localization by leveraging the reported optical cavities as efficient phonon transducers and sources [76]. As such, the Letter presented here offers a system to investigate the interplay between optomechanical effects and multiple scattering in unavoidably disordered systems and is a nascent experimental effort to explore localization phenomena with coupled excitations [77].

This work was supported by the Spanish Minister of Science, Innovation and Universities via the Severo Ochoa Program (Grant No. SEV-2017-0706) as well as by the CERCA Program/Generalitat de Catalunya and the EU-H2020 FET Proactive project TOCHA (No. 824140). G. A. was supported by the project RTI2018-093921-A-C44 (SMOOTH). R. C. N. acknowledges funding from the EU-H2020 research and innovation programme under the Marie Sklodowska-Curie (Grant No. 897148). P. D. gratefully acknowledges the support of a Ramon y Cajal fellowship (RYC-2015-18124) and C. M. S. T. acknowledges the support of the national project SIP (Grant No. PGC2018-104333-BI00). M. A. and S. S. gratefully acknowledge funding from the Villum Foundation Young Investigator Program (Grant No. 13170), the Danish National Research Foundation (Grant No. DNRF147—NanoPhoton), Innovation Fund Denmark (Grant No. 0175-00022—NEXUS), and Independent Research Fund Denmark (Grant No. 0135-00315—VAFL).

*pd.garcia@csic.es

[1] C. V. Raman, Indian J. Phys. **2**, 387 (1928).
[2] L. Brillouin, Ann. Phys. (N.Y.) **9**, 88 (1922).
[3] F. Grosse, E. A. Muljarov, and R. Zimmermann, Phonons in quantum dots and their role in exciton dephasing, in *Semiconductor Nanostructures* (Springer, Berlin, Heidelberg, 2008).
[4] C. Bond, D. Brown, A. Freise, and K. A. Strain, Living Rev. Relativity **19**, 3 (2016).

[5] J. Jabczyski, W. Zendzian, and J. Kwiatkowski, Opt. Express **14**, 2184 (2006).
[6] W. Li and S. Fan, Opt. Photonics News **30**, 32 (2019).
[7] T. Westphal, H. Hepach, J. Pfaff, and M. Aspelmeyer, Nature (London) **591**, 225 (2021).
[8] B. Gurlek, V. Sandoghdar, and D. Martin-Cano, Phys. Rev. Lett. **127**, 123603 (2021).
[9] M. Aspelmeyer, T. J. Kippenberg, and F. Marquardt, Rev. Mod. Phys. **86**, 1391 (2014).
[10] M. Minkov and V. Savona, Sci. Rep. **4**, 5124 (2014).
[11] W. Cai and W. D. Nix, *Imperfections in Crystalline Solids*, MRS-Cambridge Materials Fundamentals (Cambridge University Press, Cambridge, England, 2016).
[12] T. Baba, Nat. Photonics **2**, 465 (2008).
[13] M. G. Scullion, Y. Arita, T. F. Krauss, and K. Dholakia, Optica **2**, 816 (2015).
[14] S. Hughes, L. Ramunno, J. F. Young, and J. E. Sipe, Phys. Rev. Lett. **94**, 033903 (2005).
[15] J. Topolancik, B. Ilic, and F. Vollmer, Phys. Rev. Lett. **99**, 253901 (2007).
[16] V. Savona, Phys. Rev. B **83**, 085301 (2011).
[17] See Supplemental Material at http://link.aps.org/supplemental/10.1103/PhysRevLett.130.043802; Sec. S2, details on the fabrication process, which includes Refs. [18,19]; S3. 2: for details on the mode volume estimation, which includes Refs. [20–23]; S4. 4 for an analysis of the transmission fluctuations and the extraction of the dimensionless conductance in both the Anderson-localization and the Fabry-Prot regimes, which includes Refs. [24–26]; and Sec. S1. 2 for numerical simulations to extract ξ, which includes Refs. [27,28]..
[18] V. T. H. Nguyen, C. Silvestre, P. Shi, R. Cork, F. Jensen, J. Hübner, K. Ma, P. Leussink, M. de Boer, and H. Jansen, ECS J. Solid State Sci. Technol. **9**, 024002 (2020).
[19] V. T. H. Nguyen, F. Jensen, J. Hübner, E. Shkondin, R. Cork, K. Ma, P. Leussink, W. D. Malsche, and H. Jansen, J. Vac. Sci. Technol. B **39**, 032201 (2021).
[20] M. Notomi, Rep. Prog. Phys. **73**, 096501 (2010).
[21] P. Lalanne, W. Yan, K. Vynck, C. Sauvan, and J.-P. Hugonin, Laser Photonics Rev. **12**, 1700113 (2018).
[22] M. Charbonneau-Lefort, E. Istrate, M. Allard, J. Poon, and E. H. Sargent, Phys. Rev. B **65**, 125318 (2002).
[23] M. Patterson, S. Hughes, S. Combrié, N.-V.-Q. Tran, A. De Rossi, R. Gabet, and Y. Jaouën, Phys. Rev. Lett. **102**, 253903 (2009).
[24] A. Chabanov, M. Stoytchev, and A. Z. Genack, Nature (London) **404**, 850 (2000).
[25] M. C. W. van Rossum and Th. M. Nieuwenhuizen, Rev. Mod. Phys. **71**, 313 (1999).
[26] G. Arregui, D. Navarro-Urrios, N. Kehagias, C. M. Sotomayor Torres, and P. D. García, Phys. Rev. B **98**, 180202(R) (2018).
[27] P. D. García, G. Kirsanske, A. Javadi, S. Stobbe, and P. Lodahl, Phys. Rev. B **96**, 144201 (2017).
[28] A. Baron, S. Mazoyer, W. Smigaj, and P. Lalanne, Phys. Rev. Lett. **107**, 153901 (2011).
[29] B. Wang, S. Mazoyer, J. P. Hugonin, and P. Lalanne, Phys. Rev. B **78**, 245108 (2008).
[30] A. Di Falco, M. Massari, M. G. Scullion, S. A. Schulz, F. Romanato, and T. F. Krauss, IEEE Photonics J. **4**, 1536 (2012).
[31] P. D. García and P. Lodahl, Ann. Phys. (Amsterdam) **529**, 1600351 (2017).
[32] P. W. Anderson, Phys. Rev. **109**, 1492 (1958).
[33] J. Topolancik, B. Ilic, and F. Vollmer, Appl. Phys. Lett. **91**, 201102 (2007).
[34] A. Faraon, I. Fushman, D. Englund, N. Stoltz, P. Petroff, and J. Vuckovic, Opt. Express **16**, 12154 (2008).
[35] H. S. Dutta, A. K. Goyal, V. Srivastava, and S. Pal, Photonics Nanostructures: Fundam. Appl. **20**, 41 (2016).
[36] J. Fait, S. Putz, G. Wachter, J. Schalko, U. Schmid, M. Arndt, and M. Trupke, Appl. Phys. Lett. **119**, 221112 (2021).
[37] J. Gomis-Bresco, D. Navarro-Urrios, M. Oudich, S. El-Jallal, A. Griol, D. Puerto, E. Chavez, Y. Pennec, B. Djafari-Rouhani, F. Alzina, A. Martínez, and C. M. Sotomayor Torres, Nat. Commun. **5**, 4452 (2014).
[38] M. Okano, T. Yamada, J. Sugisaka, N. Yamamoto, M. Itoh, T. Sugaya, K. Komori, and M. Mori, J. Opt. **12**, 075101 (2010).
[39] M. W. Lee, C. Grillet, C. G. Poulton, C. Monat, C. L. C. Smith, E. Mägi, D. Freeman, S. Madden, B. Luther-Davies, and B. J. Eggleton, Opt. Express **16**, 13800 (2008).
[40] P. D. García, G. Kiršanské, A. Javadi, S. Stobbe, and P. Lodahl, Phys. Rev. B **96**, 144201 (2017).
[41] C. M. Patil, G. Arregui, M. Mechlenborg, X. Zhou, H. Alaeian, P. D. García, and S. Stobbe, Opt. Express **30**, 12565 (2022).
[42] S. Smolka, H. Thyrrestrup, L. Sapienza, T. B. Lehmann, K. R. Rix, L. S. Froufe-Pérez, P. D. García, and P. Lodahl, New J. Phys. **13**, 063044 (2011).
[43] J. P. Vasco and S. Hughes, Phys. Rev. B **95**, 224202 (2017).
[44] J. D. Hood, A. Goban, A. Asenjo-Garcia, M. Lu, S. P. Yu, D. E. Chang, and H. J. Kimble, Proc. Natl. Acad. Sci. U.S.A. **113**, 10507 (2016).
[45] C. Koos, P. Vorreau, T. Vallaitis, P. Dumon, W. Bogaerts, R. Baets, B. Esembeson, I. Biaggio, T. Michinobu, F. Diederich, W. Freude, and J. Leuthold, Nat. Photonics **3**, 216 (2009).
[46] J. Jágerská, H. Zhang, Z. Diao, N. Le Thomas, and R. Houdré, Opt. Lett. **35**, 2523 (2010).
[47] X. Luan, Y. Huang, Y. Li, J. F. McMillan, J. Zheng, S.-W. Huang, P.-C. Hsieh, T. Gu, D. Wang, A. Hati, D. A. Howe, G. Wen, M. Yu, G. Lo, D.-L. Kwong, and C. W. Wong, Sci. Rep. **4**, 6842 (2014).
[48] M. Winger, T. D. Blasius, T. P. Mayer Alegre, A. H. Safavi-Naeini, S. Meenehan, J. Cohen, S. Stobbe, and O. Painter, Opt. Express **19**, 24905 (2011).
[49] A. H. Safavi-Naeini, T. P. Mayer Alegre, M. Winger, and O. Painter, Appl. Phys. Lett. **97**, 181106 (2010).
[50] M. L. Gorodetksy, A. Schliesser, G. Anetsberger, S. Deleglise, and T. J. Kippenberg, Opt. Express **18**, 23236 (2010).
[51] A. Pitanti, J. M. Fink, A. H. Safavi-Naeini, J. T. Hill, C. U. Lei, A. Tredicucci, and O. Painter, Opt. Express **23**, 3196 (2015).
[52] R. Leijssen, G. R. La Gala, L. Freisem, J. T. Muhonen, and E. Verhagen, Nat. Commun. **8**, ncomms16024 (2017).
[53] K. E. Grutter, M. I. Davano, and K. Srinivasan, Optica **2**, 994 (2015).
[54] A. H. Safavi-Naeini and O. Painter, Opt. Express **18**, 14926 (2010).

[55] H. Jansen, M. de Boer, R. Wiegerink, N. Tas, E. Smulders, C. Neagu, and M. Elwenspoek, Microelectron. Eng. **35**, 45 (1997).
[56] M. Eichenfield, R. Camacho, J. Chan, K. J. Vahala, and O. Painter, Nature (London) **459**, 550 (2009).
[57] K. J. Vahala, Phys. Rev. A **78**, 023832 (2008).
[58] L. Sapienza, H. Thyrrestrup, S. Stobbe, P. D. García, S. Smolka, and P. Lodahl, Science **327**, 1352 (2010).
[59] H. Thyrrestrup, S. Smolka, L. Sapienza, and P. Lodahl, Phys. Rev. Lett. **108**, 113901 (2012).
[60] J. Liu, P. D. García, S. Ek, N. Gregersen, T. Suhr, M. Schubert, J. Mørk, S. Stobbe, and P. Lodahl, Nat. Nanotechnol. **9**, 285 (2014).
[61] J. Bertolotti, E. G van Putten, C. Blum, A. Lagendijk, W. L Vos, and A. P. Mosk, Nature (London) **491**, 232 (2012).
[62] K. Watanabe, H.-Y. Wu, J. Xavier, L. T. Joshi, and F. Vollmer, Small **18**, 2107597 (2022).
[63] M. Rafayelyan, J. Dong, Y. Tan, F. Krzakala, and S. Gigan, Phys. Rev. X **10**, 041037 (2020).
[64] S. Gentilini and C. Conti, Phys. Rev. A **91**, 043813 (2015).
[65] M. Albrechtsen, B. Vosoughi Lahijani, R. E. Christiansen, V. T. H. Nguyen, L. N. Casses, S. E. Hansen, N. Stenger, O. Sigmund, H. Jansen, J. Mørk, and S. Stobbe, Nat. Commun. **13**, 6281 (2022).
[66] F. J. García de Abajo and V. Di Giulio, ACS Photonics **8**, 945 (2021).
[67] J.-B. Béguin, Z. Qin, X. Luan, and H. J. Kimble, Proc. Natl. Acad. Sci. U.S.A. **117**, 29422 (2020).
[68] X. Zhang, T. Lin, F. Tian, H. Du, Y. Zou, F. S. Chau, and G. Zhoub, Appl. Phys. Lett. **112**, 153502 (2018).
[69] U. Kemiktarak, M. Durand, M. Metcalfe, and J. Lawall, Phys. Rev. Lett. **113**, 030802 (2014).
[70] L. Mercadé, K. Pelka, R. Burgwal, A. Xuereb, A. Martínez, and E. Verhagen, Phys. Rev. Lett. **127**, 073601 (2021).
[71] R. C. Ng, P. Nizet, D. Navarro-Urrios, G. Arregui, M. Albrechtsen, P. D. García, S. Stobbe, C. M Sotomayor-Torres, and G. Madiot, arXiv:2210.16370.
[72] M. J. Weaver, F. Buters, F. Luna, H. Eerkens, K. Heeck, S. de Man, and D. Bouwmeester, Nat. Commun. **8**, 824 (2017).
[73] A. H. Safavi-Naeini, J. T. Hill, S. Meenehan, J. Chan, S. Gröblacher, and O. Painter, Phys. Rev. Lett. **112**, 153603 (2014).
[74] G. Madiot, R. C Ng, G. Arregui, O. Florez, M. Albrechtsen, S. Stobbe, P. D García, and C. M Sotomayor-Torres, arXiv:2206.06913.
[75] O. Florez, G. Arregui, M. Albrechtsen, R. C. Ng, J. Gomis-Bresco, S. Stobbe, C. M. Sotomayor-Torres, and P. D. García, Nat. Nanotechnol. **17**, 947 (2022).
[76] P. D. García, R. Bericat-Vadell, G. Arregui, D. Navarro-Urrios, M. Colombano, F. Alzina, and C. M. Sotomayor-Torres, Phys. Rev. B **95**, 115129 (2017).
[77] T. F. Roque, V. Peano, O. M. Yevtushenko, and F. Marquardt, New J. Phys. **19**, 013006 (2017).